


# Molecular orbital effect in above-threshold ionization of vinyl bromide induced by strong laser fields

Qi Chen(陈淇), Yang Liu(刘洋), Wei Yang(杨威), Di Liu(刘迪), Hang Lv(吕航), Bing Yan(闫冰), and Haifeng Xu(徐海峰)

**Citation:**Chin. Phys. B, 2026, 35 (**4**): 043303. DOI: 10.1088/1674-1056/ae4465
http://cpb.iphy.ac.cn; http://iopscience.iop.org/cpb

**What follows is a list of articles you may be interested in**

---

## Time-dependent quantum wave packet simulation for strong laser-induced molecular dynamics in multiple electronic states of $H_2$ molecules

Jin-Peng Ma(马金鹏), Xiao-Qing Hu(胡晓青), Yong Wu(吴勇), and Jian-Guo Wang(王建国)
Chin. Phys. B, 2025, 34 (**10**): 103301. DOI: 10.1088/1674-1056/adf319

## Effect of laser polarization on strong-field ionization and fragmentation of nitrous oxide molecules

Rui Wang(王瑞), Shi-Wen Zhang(张世文), Yang Liu(刘洋), Tian Sun(孙添), Hang Lv(吕航), Hai-Feng Xu(徐海峰)
Chin. Phys. B, 2019, 28 (**5**): 053301. DOI: 10.1088/1674-1056/28/5/053301

## Enhanced ionization of vibrational hot carbon disulfide molecules in strong femtosecond laser fields

Wan-Long Zuo(左万龙), Hang Lv(吕航), Hong-Jing Liang(梁红静), Shi-Min Shan(单石敏), Ri Ma(马日), Bing Yan(闫冰), Hai-Feng Xu(徐海峰)
Chin. Phys. B, 2018, 27 (**6**): 063301. DOI: 10.1088/1674-1056/27/6/063301

## Rydberg excitation of neutral nitric oxide molecules instrong UV and near-IR laser fields

Lv Hang (吕航), Zhang Jun-Feng (张军峰), Zuo Wan-Long (左万龙), Xu Hai-Feng (徐海峰), Jin Ming-Xing (金明星), Ding Da-Jun (丁大军)
Chin. Phys. B, 2015, 24 (**6**): 063303. DOI: 10.1088/1674-1056/24/6/063303

## Low-energy structure in the ionization of argon: Comparison of experiment with theory

Feng Li-Qiang (冯立强), Chu Tian-Shu (楚天舒), Wang Li (王利)
Chin. Phys. B, 2013, 22 (**2**): 023302. DOI: 10.1088/1674-1056/22/2/023302

---

**SPECIAL TOPIC — Ultrafast physics in atomic, molecular and optical systems**

# Molecular orbital effect in above-threshold ionization of vinyl bromide induced by strong laser fields

Qi Chen(陈淇), Yang Liu(刘洋), Wei Yang(杨威), Di Liu(刘迪), Hang Lv(吕航)†, Bing Yan(闫冰), and Haifeng Xu(徐海峰)‡

*Institute of Atomic and Molecular Physics, Jilin University, Changchun* 130012, *China*

(Received 3 February 2026; revised manuscript received 3 February 2026; accepted manuscript online 11 February 2026)

Ionization is a fundamental process that may induce a variety of highly nonlinear physical phenomena in strong femtosecond laser fields. Compared to that of atoms, strong-field ionization (SFI) of polyatomic molecules is far from being understood because of their diverse geometric and orbital structures. In this study, we experimentally investigate SFI of the vinyl bromide ($C_2H_3Br$) molecule in near ultraviolet and near-infrared strong laser fields employing the electron velocity map imaging (VMI) method. The distinct above-threshold ionization (ATI) structure of the molecule is clearly observed in both strong laser fields. The electron kinetic energy as well as the angular distributions is derived from the electron VMI measurements, and their dependence on the laser intensity is investigated and discussed. Analysis reveals that owing to the small energy difference between the low-lying electronic orbitals of the $C_2H_3Br$ molecule, multiple orbital effect plays a pivotal role in the SFI of the molecule. The present study adds our knowledge on SFI and ATI of the $C_2H_3Br$ molecule, and sheds some light on the interaction of polyatomic molecules with ultrafast strong laser fields.

**Keywords:** above threshold ionization, strong laser field, molecular orbital effect, vinyl bromide

**PACS:** 33.80.Eh

**DOI:** 10.1088/1674-1056/ae4465 **CSTR:** 32038.14.CPB.ae4465

## 1. Introduction

When an atom or a molecule interacts with femtosecond strong laser fields, a variety of nonlinear physical phenomena occur, including nonsequential double/multiple ionization, high-order above threshold ionization, high-order harmonic generation and neutral Rydberg state excitation.[1–8] Ionization is often viewed as the most fundamental step in strong-field physics, since the freed electron could induce different processes under the interaction of the laser electric field and the Coulomb potential. During the past decades, increasing interest has focused on the strong-field ionization (SFI) of atoms, paving the way for many new research topics such as ultrafast electron diffraction, ultrafast holography, coherent control, attosecond pulse generation, and so on.[9–12]

Compared to atoms, molecules exhibit diverse geometric structures, complex electronic orbitals, and additional nuclear degree-of-freedom, thus leading to much more complicated physical processes when interacting with strong laser fields. There are many intriguing phenomena with regard to SFI of molecules, for instance, excitation and dissociation,[13,14] enhanced and suppressed ionization,[15] multi-center and multi-orbital effects,[16,17] alignment and orientation,[18] etc. Various studies have shown that in addition to the laser parameters (e.g., central wavelength, pulse duration, laser intensity, polarization state and carrier envelope phase),[19–26] the geometric and electronic orbital structures are also essential to understand SFI and related physical processes of molecules.[27,28] Particularly, owing to the small energy difference of molecular orbitals especially for polyatomic molecules, not only the highest occupied molecular orbital (HOMO) but also lower-lying orbitals (HOMO-1, HOMO-2, etc.) would contribute to strong-field physical processes, facilitating diverse structure-dependent effects including multiple channels, electron correlations and quantum interferences.[27–31] Furthermore, the direct and indirect ionization pathways to excited cationic states in SFI of molecules are identified, revealing that the energy gap between non-dissociative and dissociative states plays a critical role in governing the yield of excited-state ionization.[32,33]

Here, we focus on SFI of the $C_2H_3Br$ molecule in femtosecond strong laser fields with central wavelength near ultraviolet (UV, 400 nm) or near infrared (NIR, 800 nm). $C_2H_3Br$ is a typical molecule which has several molecular orbitals close in energy and located on either of the two distinct parts (i.e., the Br atom and the $C_2H_3$ radical), allowing possible coherent excitation of multiple orbitals during strong field ionization.[34] Most of the studies available in the literature focused on spectroscopic experiments and *ab initio* calculations to investigate the structure, spectroscopy, and dissociation of electronic states of both the $C_2H_3Br$ molecule and

†Corresponding author. E-mail: lvhang0811@jlu.edu.cn

‡Corresponding author. E-mail: xuhf@jlu.edu.cn

© 2026 Chinese Physical Society and IOP Publishing Ltd. All rights, including for text and data mining, AI training, and similar technologies, are reserved.

its cations.[35–41] However, our knowledge on the interaction of the titled molecule with ultrafast strong laser fields is quite limited, which has been investigated in only a few studies so far. Castillejo *et al.* employed a time-of-flight spectrometer to investigate the angular distributions of multiply charged atomic ions generated through dissociative ionization and Coulomb explosion of $C_2H_3Br$ molecules in strong 800-nm laser fields, indicating the anisotropic ejection of fragment ions which could be attributed to the dependence of SFI on the orientation of the molecular transition dipole moment relative to the laser polarization direction.[42] This is further demonstrated by a recent study of Liu *et al.*, which also compared the ionization and dissociation of the molecules in NIR laser fields and to that in 400-nm laser fields, showing different mechanisms of SFI in different laser fields.[43] Moreover, by employing SFI as the pump step to prepare vinyl bromide ions, the ultrafast dynamics of the cationic states were studied in a couple of studies, using either time-resolved attosecond transient absorption spectroscopy[44] or photofragmentation detection[45] as the probe, implying the simultaneous excitation of multiple orbitals of the molecules in strong laser fields.

As a fundamental phenomenon in strong-field physics, ATI has found broad applications in many areas, such as probing electron orbital symmetry and molecular structure imaging, thus it has been widely investigated in atoms. However, ATI of polyatomic molecules remains largely unexplored, and that of the titled molecule has not been experimentally observed yet. In this study, by employing the electron VMI method, we observe ATI of the $C_2H_3Br$ molecule in linearly polarized near UV and NIR strong laser fields. The electron kinetic energy (eKE) and photoelectron angular distributions (PADs) are derived and analyzed for both strong laser fields with different laser intensities. The contributions of multiple molecular orbitals in SFI of the $C_2H_3Br$ molecule are clearly identified, and the relative contributions of multiple orbitals to the ionization yield are retrieved and analyzed. The underlying physics of ATI of the $C_2H_3Br$ molecule is discussed based on the experimental observations.

## 2. Experimental setup

We employ a home-built VMI system to investigate ATI of the $C_2H_3Br$ molecule in strong laser fields. The laser system (Astrella, Coherent) used in the experiments is a Ti:sapphire chirped-pulse amplified laser with a central wavelength of 800 nm, a transform-limited pulse width of 35 fs, a repetition rate of 1 kHz and a maximum pulse energy of 7 mJ. The 400-nm laser pulses are obtained by frequency doubling of the fundamental output of the laser system using a BBO crystal. A half-wave plate and a Glan prism are inserted into the laser beam to change the laser intensity. Before it is introduced into the vacuum chamber to interact with the molecular beam, the laser beam is focused by a thin lens with a focal length of 25 cm. The peak intensity of the focused laser pulse is calibrated by comparing the measured saturation intensity of ionization of Ar with that calculated by the Ammosov–Delone–Krainov (ADK) model[46] or Perelomov–Popov–Terent'ev (PPT) theory[47] for 800-nm or 400-nm laser fields, respectively. The $C_2H_3Br$ gas sample is introduced directly into the chamber through a leak valve with the stagnation pressure of 1 atm. With gas injection, the pressure in the laser-molecule interaction chamber is maintained at about $1 \times 10^{-5}$ Pa. Ionized electrons after the molecule interacts with the focused laser beam are detected by a dual microchannel plates (MCP) detector at the end of the flight (about 20 cm). A phosphor screen is coupled to the MCP detector, and the image is recorded by a charge-coupled device (CCD) camera. The inverse-Abel transformation procedure is utilized to reconstruct the three-dimensional photoelectron distribution. The eKE is calibrated by ATI of Kr atoms in either near-UV or NIR strong laser fields, and the full width at half maximum of the atomic ATI peak is about 0.6 eV @ 7 eV.

## 3. Results and discussion

In our electron VMI study, the laser intensity is used in the range of 1–10 TW/cm$^2$ and 7–40 TW/cm$^2$ for the near UV and NIR laser fields, respectively. The corresponding Keldysh parameter ($\gamma = \sqrt{\frac{I_P}{2U_P}}$,[48] where $I_P = 9.82$ eV is the ionization potential,[49] and $U_P = I/4\omega^2$ is the ponderomotive energy) is within $5.7 < \gamma < 18$ and $1.4 < \gamma < 3.3$, respectively. Thus, the multiphoton ionization (MPI) instead of tunneling ionization would be dominant in the ionization of the $C_2H_3Br$ molecules in either 400-nm or 800-nm laser fields. In Fig. 1(a), we present a typical photoelectron image of the $C_2H_3Br$ molecule measured in a linearly polarized 400-nm laser field with an intensity of 3 TW/cm$^2$. Distinct rings are observed with the maximal population along the polarization direction of the laser field. The eKE distribution up to 15 eV is derived from the image as presented in Fig. 1(b). It can be seen that eKE peaks appear every $\sim 3.0$ eV, the interval that is close to the photon energy of the 400-nm laser field $h\nu_{400\text{-nm}} = 3.1$ eV. This observation indicates that the ATI process of the $C_2H_3Br$ molecule occurs in strong 400-nm laser fields, i.e., the molecules absorb more than the minimum number of photons required for ionization. For the $C_2H_3Br$ molecule, at least four $h\nu_{400\text{-nm}}$ photons are required for ionization. The dominant feature at low- eKE below 3 eV is assigned as four-photon ionization (FPI) of the $C_2H_3Br$ molecule. The structure observed at eKE near 6 eV, 9 eV and 12 eV would be due to the first-, the second- and the third-order ATI of the $C_2H_3Br$ molecule, respectively, that is, absorption of one, two and three additional photons to ionize the molecule.

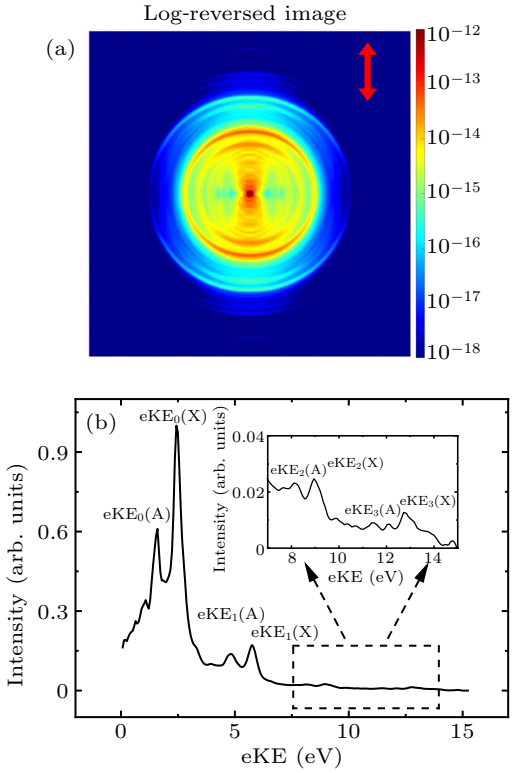



**Fig. 1.** (a) Log-reversed photoelectron VMI of $C_2H_3Br$ molecule in 400-nm laser field with an intensity of 3 TW/cm$^2$. The red arrow indicates the laser polarization direction. (b) The corresponding eKE distribution. The inset shows an enlarged view of the 7–15 eV region.

Interestingly, two well-separated peaks are clearly observed for FPI and each order of ATI, as shown in Fig. 1(b). This observation strongly indicates the multi-orbital effect in SFI of the $C_2H_3Br$ molecule. It is well-known that for the $C_2H_3Br$ molecule, the energies of low-lying molecular orbitals are close,[37,45] leading to possible populations in different cationic electronic states upon ionization in strong laser fields. We employ CASPT2 calculations on the geometric structures, the potential energy curves along the C–Br bond, and the electronic configurations of the neutral and cationic ground electronic states (see supplementary material). The energy difference between the HOMO and HOMO-1 orbitals is calculated to be 1.1 eV, which is in line with previous measurements (the adiabatic $I_P$ for HOMO is 9.82 eV, while that for HOMO-1 is 10.90 eV[49]). For MPI from the HOMO and HOMO-1 orbitals in the 400-nm laser field, the eKEs are 2.58 eV and 1.50 eV, respectively, leaving the cation in the ground X-state and the first-excited A-state. The experimentally observed eKE peaks shown in Fig. 1(b) (2.43 eV and 1.60 eV labeled as eKE$_0$(X) and eKE$_0$(A), respectively) are well consistent with these expected values. Consequently, the ATI process from different orbitals leads to a pair of eKE peaks at an interval of 3 eV, namely, eKE$_i$(X) and eKE$_i$(A) as illustrated in Fig. 1(b).

To further elucidate the molecular orbital effect in SFI of the $C_2H_3Br$ molecule, we present in Figs. 2(a) and 2(b) the PADs for FPI (eKE$_0$(X) and eKE$_0$(A)) and the 1$^{st}$-order ATI (eKE$_1$(X) and eKE$_1$(A)) respectively. It can be seen from the figures that the PADs have strong anisotropic character for both FPI and ATI. Close inspection reveals distinctly different PADs for ionization from different orbitals. For either FPI or ATI, the electron ionized from HOMO-1 (eKE$_0$(A) and eKE$_1$(A)) presents a PAD with maximum along the laser polarization direction (0° and 180°); while the PADs for the ionization from HOMO (eKE$_0$(X) and eKE$_1$(X)) exhibit a butterfly-like structure with the maximum population at the direction that obviously deviates (approximately 25°) from the laser polarization. Moreover, compared to that for HOMO-1, the PAD for HOMO is more anisotropically pronounced with less population in the direction perpendicular to the laser polarization (90°).

The different behaviors of PADs of eKE$_i$(X) and eKE$_i$(A) shown in Figs. 2(a) and 2(b) could be attributed to the different structures of HOMO and HOMO-1 of the $C_2H_3Br$ molecule. Although the $C_2H_3Br$ molecules in the experiment are randomly oriented, the molecules are mainly ionized when their C–Br axis is aligned along the laser polarization direction due to the geometric alignment.[50] Owing to this, the electron is preferentially ionized from the regions with the largest magnitude distribution of electronic clouds; therefore, the angular distribution could reflect the structure of the molecular orbitals from which the electron is removed. As shown in Fig. 2(c), the HOMO of $C_2H_3Br$ resembles a $\pi$-character orbital, which is similar to that of $CO_2$. The electron density of HOMO is located between the C–Br atoms. Both the molecular plane and the plane perpendicular to the C–Br bond are nodal planes for HOMO. On the other hand, there is only one nodal plane of HOMO-1 (Fig. 2(d)), which is perpendicular to the C–Br bond. Therefore, the electron ionized from HOMO would prefer to eject in the direction which deviates from the laser polarization and the intensity at 90° would be reduced, as we have observed in the PADs shown in Fig. 2. These observations demonstrate the multi-orbital effect in SFI of the $C_2H_3Br$ molecule.

We further investigate the laser-intensity dependent FPI and ATI from different molecular orbitals of the $C_2H_3Br$ molecule. Figures 3(a)–3(d) present photoelectron images recorded under the laser intensity of 1 TW/cm$^2$, 3 TW/cm$^2$, 7 TW/cm$^2$ and 10 TW/cm$^2$, respectively. The corresponding eKE distributions are presented in Fig. 3(e). While similar distinct structures are observed at different laser intensities, the relative yields for eKE$_i$(X) and eKE$_i$(A) vary. As shown in Fig. 3(e), the signal intensity for the eKE$_i$(X) peak gradually increases while that for eKE$_i$(A) decreases ($i$ = 0–3) upon increasing the laser intensity. This observation is more clearly elucidated in Fig. 3(f), in which the intensity-dependent yield ratio of eKE$_i$(A)/eKE$_i$(X) is presented. For either FPI or the 1$^{st}$-order ATI, the ratio eKE$_0$(A)/eKE$_0$(X) or eKE$_1$(A)/eKE$_1$(X) gradually decreases with increasing laser intensity.

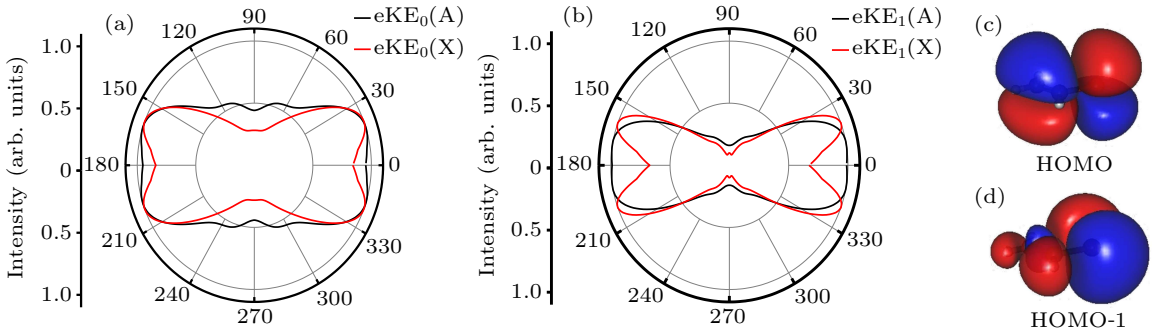



**Fig. 2.** Photoelectron angular distributions for FPI (a) and the first-order ATI (b) in 400-nm laser fields. (c) and (d) The structures of HOMO and HOMO-1 of $C_2H_3Br$ molecule calculated using the internally contracted complete active space second-order perturbation theory (CASPT2) method.

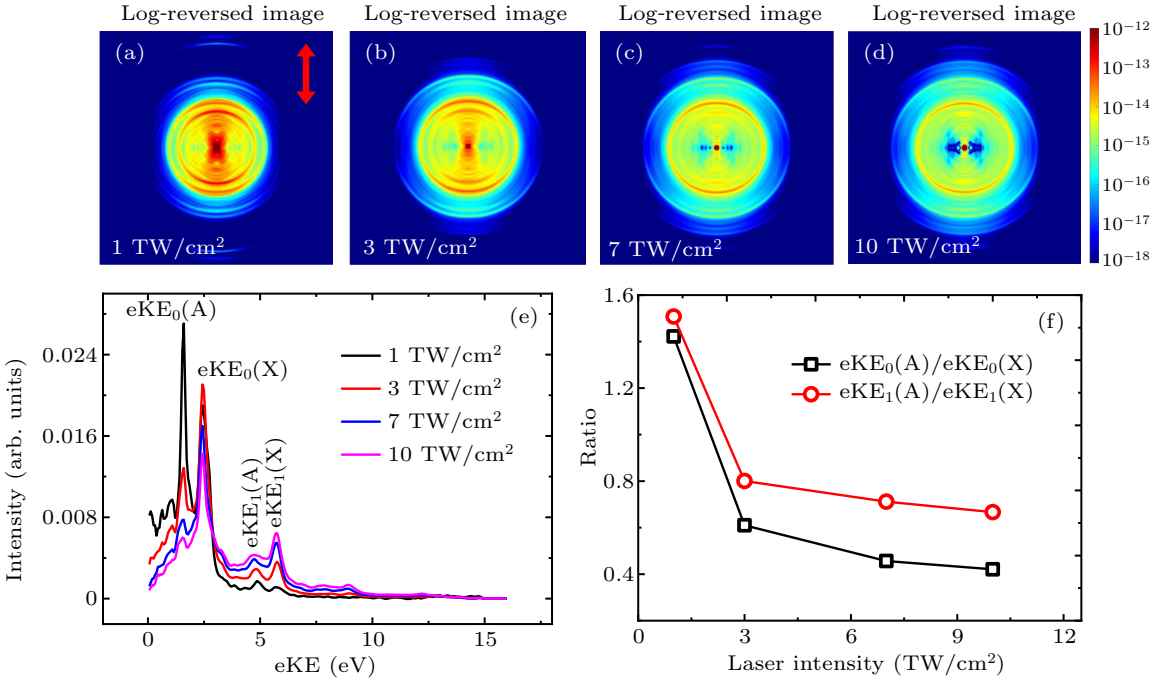



**Fig. 3.** Log-reversed photoelectron VMI in 400-nm laser field with laser intensity of (a) 1 TW/cm$^2$, (b) 3 TW/cm$^2$, (c) 7 TW/cm$^2$ and (d) 10 TW/cm$^2$. (e) The eKE distributions at different laser intensities. (f) Ratios of the peaks eKE$_0$(A)/eKE$_0$(X) (black squares) and eKE$_1$(A)/eKE$_1$(X) (red circles) as a function of the laser intensity. See text for details.

To investigate this phenomenon, we evaluate the relative contributions to the total ionization rate from the HOMO and HOMO-1 orbitals (see supplementary material). With the calculated PECs and FCFs, we estimate the ratio to be $\sim 1.50$, explaining that the yield for the cationic A-state is higher than that for the X-state at low laser intensity (1 TW/cm$^2$), as we have observed shown in Fig. 3(d). As the laser intensity increases, perturbation treatment is no longer valid, the ionization rate $\Gamma(R)$ would strongly rely on the ionization potential $I_P(R)$, which varies upon the internuclear distance $R$ for a molecule.[51] Then we estimate the ratio eKE(A)/eKE(X) to be $\sim$0.53 at 10 TW/cm$^2$, much smaller than that at low laser intensity, which could be attributed to higher $I_P$ of HOMO-1 than that of HOMO. The observed decrease of the ratio eKE(A)/eKE(X) in Fig. 3(d) indicates the ionization mechanism of $C_2H_3Br$ changes from the perturbative to the nonperturbative MPI as the laser intensity is increased.

We now turn to discuss the ionization of the $C_2H_3Br$ molecule in the 800-nm laser fields. Figure 4(a) presents the photoelectron image of the $C_2H_3Br$ molecule after irradiated by the 800-nm femtosecond laser with a peak intensity of 7 TW/cm$^2$. Distinct structures are observed along the laser polarization direction, exhibiting near-uniform spacing in energy and gradually decreasing in intensity. The corresponding eKE distribution is shown in Fig. 4(b), with a series of peaks identified and indicated as $E_i$ ($i = 1$–8) in the figure. The PAD at each eKE peak is presented in Fig. 4(c).

The distinct structure in the VMI image and the eKE peaks $E_i$ ($i = 1$–8) can be unambiguously assigned to ATI of the $C_2H_3Br$ molecule induced by the strong NIR laser fields, since the peaks exhibit uniform energy spacing with an interval approximately equal to the photon energy of the laser ($h\nu_{800\text{-nm}} = 1.55$ eV). It should be mentioned that ionization from different MOs, i.e., HOMO and HOMO-1 as we have discussed in the above section, is not clearly observed in strong field ionization by the NIR laser fields. Consider-

ing the fact that the energy difference between HOMO and HOMO-1 (1.10 eV) is close to $h\nu_{800\text{-nm}}$, and the $U_P$ shift is much larger in the 800-nm laser fields ($U_P \propto I\lambda^2$, which is 0.42 eV at 7 TW/cm$^2$), the eKE peaks of the ionization from the two MOs will be buried in the ATI structure and cannot be distinguished in the present study. One may note that there is a shoulder in each $E_i$ peak as shown in Fig. 4(b). Tentative assignment of these shoulders is presented in supplementary material, the results of which indicate that these features could be attributed to ionization from different MOs.

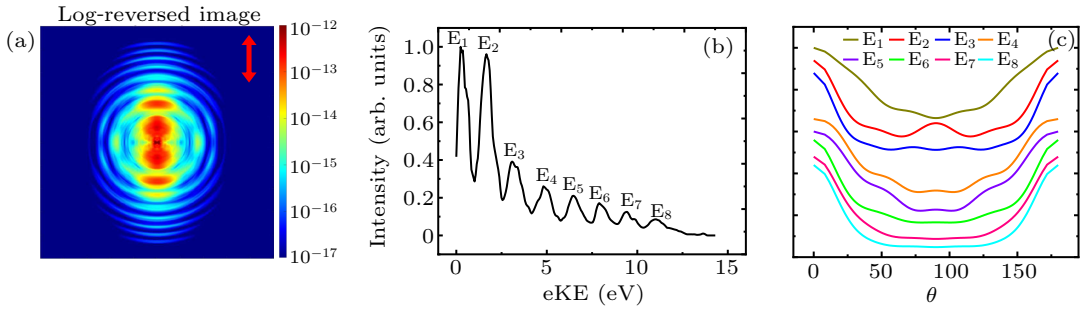



**Fig. 4.** (a) Log-reversed photoelectron VMI after irradiated by 800-nm laser field. The corresponding eKE distribution (b) and photoelectron angular distribution of the ATI peaks (c). The laser intensity is 7 TW/cm$^2$.

The PADs shown in Fig. 4(c) indicate that the photoelectron is preferred to emit along the laser polarization (at 0° and 180°) and different structure features are visible for low-order ATI peaks $E_1$–$E_5$ with local maxima at other angles. Specifically along the direction perpendicular to the laser polarization (90°), the photoelectron yield alternates between local minima and maxima as the ATI order increases. This observation in the $C_2H_3Br$ molecule is very similar to those of atoms widely studied in the literature.[52–55] For the $C_2H_3Br$ molecule, at least seven $h\nu_{800\text{-nm}}$ photons are needed for the first ATI peak $E_1$, and one additional photon is absorbed with successively increasing the order of ATI. As demonstrated in previous work,[56] the dominant angular momentum of the photoelectron gradually increases with the ATI order due to dipole selection rules. Consequently, the parity (odd or even) of the final state alternates accordingly. For a final state mainly composed of odd angular momenta, the probability density vanishes exactly in the plane perpendicular to the polarization direction, leading to a local minimum in the photoelectron yield at 90°. Conversely, final states with even angular momenta result in a local maximum at the same angle. Within the strong-field approximation, this alternating pattern can also be interpreted as the constructive and destructive interference between intracycle electron trajectories.[55] It can be seen that the structure gradually diminishes and the PAD turns to be more anisotropic as the order of ATI increases. For the highest order of ATI observed in the study ($E_8$), the PAD is very narrow with no population at the angle perpendicular to the laser polarization (90°).

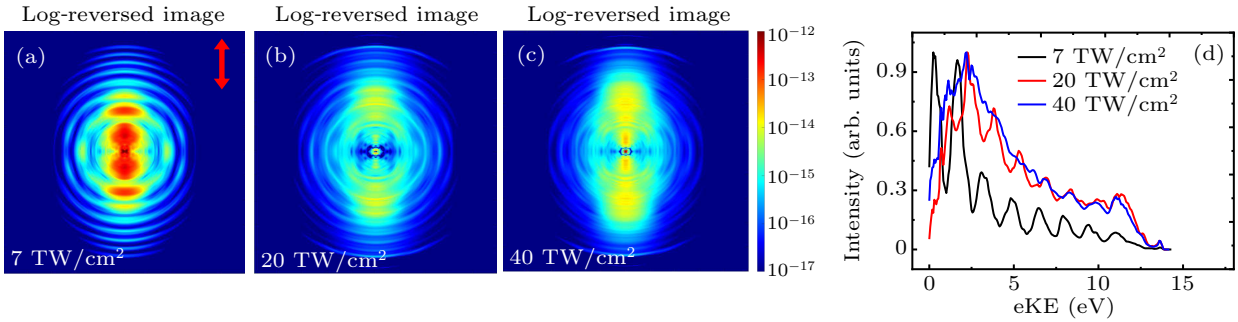



**Fig. 5.** Log-reversed photoelectron VMI after irradiated by 800-nm laser field at intensity of (a) 7 TW/cm$^2$, (b) 20 TW/cm$^2$ and (c) 40 TW/cm$^2$. (d) The corresponding eKE distributions at different laser intensities.

We further investigate ATI of the $C_2H_3Br$ molecule with varying the laser intensity. Figures 5(a)–5(c) present the photoelectron images recorded with the NIR laser intensity of 7 TW/cm$^2$, 20 TW/cm$^2$ and 40 TW/cm$^2$, respectively. While the ATI structure could be observable at different laser intensities, the feature varies significantly. When the laser intensity exceeds 20 TW/cm$^2$, the low-order ATI peaks gradually diminish, and the ATI peaks are no longer well-resolved as distinct concentric rings. The dependence of ATI on the laser intensity is also clearly illustrated in the eKE spectrum shown in Fig. 5(d). As shown in the figure, the low-order ATI peaks are suppressed when the laser intensity is higher than 20 TW/cm$^2$, and the maximum in the spectrum shifts to large eKE value with increasing the laser intensity. In addition, the distinct ATI peaks $E_1$–$E_8$ well-separated by one photon energy at 7 TW/cm$^2$ are not resolved in the spectrum at 40 TW/cm$^2$.

The suppression of the low-order ATI peaks indicates that the perturbation theory is no longer valid in strong laser fields. Moreover, the spatial Gaussian-like intensity distribution of the focused laser pulse, which induces ac-Stark shift due to the ponderomotive force in strong laser fields, would blur the well-separated ATI peaks and lead to broad unresolved eKE distribution shown in Fig. 5(d). This observation of the laser intensity dependent ATI of the $C_2H_3Br$ molecule is a common feature of the atomic ATI induced by strong NIR laser fields, which is rarely observed in molecules. Our study would add some knowledge on the interaction of polyatomic molecular systems with ultrafast strong laser fields.

## 4. Conclusion

In summary, by utilizing the electron VMI technique, we experimentally investigate ionization of the $C_2H_3Br$ molecule in linearly polarized strong near UV and NIR laser fields. Distinct ATI structure is observed in both laser fields. The eKEs and PADs are derived from the electron VMIs, and the dependence on the laser intensity is investigated. Analysis demonstrates the significant contribution of both HOMO and HOMO-1 in SFI of the molecule, which is more clearly identified in the case of the near UV laser fields, implying the multiple molecular orbital effect in strong-field physics of $C_2H_3Br$. It is indicated that more deep-lying orbitals and higher-order process would be involved in the ionization of the molecules with increasing laser intensity, which would stimulate our further studies, both experimentally and theoretically, to reveal the underlying physical mechanism about the molecular structure effect induced by ultrafast strong laser fields.

## Supplementary material

The supplementary material provides CASPT2 calculation results on the geometry and potential energy curves of $C_2H_3Br$ molecule, *R*-dependent ionization energy and ionization rate ratio of HOMO and HOMO-1 orbitals, the assignment of 800-nm ATI peak and the PADs of the low-order ATI in polar coordinates.

## Acknowledgements

This work was supported by the National Natural Science Foundation of China (Grant Nos. 12574311, 12174148, and 12274178) and the Natural Science Foundation of Jilin Province, China (Grant No. 20240101322JC).

## References

[1] Becker W, Liu X J, Ho P J and Eberly J H 2012 *Rev. Mod. Phys.* **84** 1011
[2] Figueira de Morisson Faria C and Liu X 2011 *J. Mod. Opt.* **58** 1076
[3] Becker W, Goreslavski S P, Milošević D B and Paulus G G 2018 *J. Phys. B: At. Mol. Opt. Phys.* **51** 162002
[4] Milošević D B, Paulus G G, Bauer D and Becker W 2006 *J. Phys. B: At. Mol. Opt. Phys.* **39** R203
[5] Miyazaki K and Takada H 1995 *Phys. Rev. A* **52** 3007
[6] Shen X C, Liu Y, Chen Q, Lv H and Xu H F 2022 *Acta Phys. Sin.* **71** 233202 (in Chinese)
[7] Nubbemeyer T, Gorling K, Saenz A, Eichmann U and Sandner W 2008 *Phys. Rev. Lett.* **101** 233001
[8] Zimmermann H and Eichmann U 2016 *Phys. Scr.* **91** 104002
[9] Hassan M T, Luu T T, Moulet A, Raskazovskaya O, Zhokhov P, Garg M, Karpowicz N, Zheltikov A M, Pervak V, Krausz F and Goulielmakis E 2016 *Nature* **530** 66
[10] Karasawa N, Yamada S and Kanaya H 2020 *Opt. Commun.* **473** 125941
[11] Ohmori K 2009 *Annu. Rev. Phys. Chem.* **60** 487
[12] Krausz F and Ivanov M 2009 *Rev. Mod. Phys.* **81** 163
[13] Shi H J, Liu Y, Sun T, Lv H and Xu H F 2024 *Chin. Phys. B* **33** 073301
[14] Wang S F and Wu C Y 2025 *Chin. J. Chem. Phys.* **38** 19
[15] Lv H, Zuo W L, Zhao L, Xu H F, Jin M X, Ding D J, Hu S L and Chen J 2016 *Phys. Rev. A* **93** 033415
[16] Yun H, Lee K M, Sung J H, Kim K T, Kim H T and Nam C H 2015 *Phys. Rev. Lett.* **114** 153901
[17] Shu Z, Liu M Q, Hu S L and Chen J 2020 *Opt. Express* **28** 11165
[18] Lee K F, Villeneuve D M, Corkum P B, Stolow A and Underwood J G 2006 *Phys. Rev. Lett.* **97** 173001
[19] Wu D, Wang Q Q, Cheng X H, Jin M X, Li X Y, Hu Zh and Ding D J 2007 *J. Phys. Chem. A* **111** 9494
[20] Lezius M, Blanchet V, Ivanov M Y and Stolow A 2002 *J. Chem. Phys.* **117** 1575
[21] Trushin S A, Fuß W and Schmid W E 2004 *J. Phys. B: At. Mol. Opt. Phys.* **37** 3987
[22] Campbell E E B, Hansen K, Hoffmann K, Korn G, Tchaplyguine M, Wittmann M and Hertel I V 2000 *Phys. Rev. Lett.* **84** 2128
[23] Bhardwaj V R, Rayner D M, Villeneuve D M and Corkum P B 2001 *Phys. Rev. Lett.* **87** 253003
[24] Yatsuhashi T and Nakashima N 2005 *J. Phys. Chem. A* **109** 9414
[25] Kling N G, Betsch K J, Zohrabi M, Zeng S, Anis F, Ablikim U, Jochim B, Wang Z, Kuebel M, Kling M F, Carnes K D, Esry B D and Ben-Itzhak I 2013 *Phys. Rev. Lett.* **111** 163004
[26] Bozpolat S A, Rosenberger P, Ciappina M F, Kling M F and Yavuz I 2019 *Phys. Rev. A* **100** 063409
[27] Liu Y, Yi X P, Chen Q, Sun T, Lv H, Hu S L, Becker W, Xu H F and Chen J 2024 *Photon. Res.* **12** 3033
[28] Hu S L, Hao X L, Lv H, Liu M Q, Yang T X, Xu H F, Jin M X, Ding D J, Li Q G, Li W D, Becker W and Chen J 2019 *Opt. Express* **27** 31629
[29] Itatani J, Levesque J, Zeidler D, Niikura H, Pépin H, Kieffer J C, Corkum P B and Villeneuve D M 2004 *Nature* **432** 867
[30] Yao J P, Li G H, Jia X Y, Hao X L, Zeng B, Jing C R, Chu W, Ni J L, Zhang H S, Xie H Q, Zhang C J, Zhao Z X, Chen J, Liu X J, Cheng Y and Xu Z Z 2013 *Phys. Rev. Lett.* **111** 133001
[31] Grasbon F, Paulus G G, Chin S L, Walther H, Muth-Böhm J, Becker A and Faisal F H M 2001 *Phys. Rev. A* **63** 041402
[32] Arthur Z, Péter S, Tamás R and Thomas W 2014 *J. Phys. B: At. Mol. Opt. Phys.* **47** 204023
[33] Sándor P, Arthur Z, Tamás R and Thomas W 2014 *J. Phys. B: At. Mol. Opt. Phys.* **47** 124021
[34] Du H B, Covington C, Leone S R and Varga K 2019 *Phys. Rev. A* **100** 053412
[35] Qian X M, Lau K C and Ng C Y 2004 *J. Chem. Phys.* **120** 11031
[36] Lago A F and Baer T 2006 *J. Phys. Chem. A* **110** 3036
[37] Hoxha A, Yu S Y, Locht R, Jochims H W and Leyh B 2011 *Chem. Phys.* **379** 99
[38] Chang J L and Tsao C W 2006 *Chem. Phys. Lett.* **428** 23
[39] Chuang C H, Chen C C, Wu H C and Chen Y T 2004 *Chem. Phys. Lett.* **394** 287
[40] Hoxha A, Locht R, Leyh B, Dehareng D, Hottmann K and Baumgärtel H 2000 *Chem. Phys.* **256** 239
[41] Hoxha A, Locht R, Leyh B, Dehareng D, Hottmann K, Jochims H W and Baumgärtel H 2000 *Chem. Phys.* **260** 237
[42] Castillejo M, Martin M, De Nalda R, Stelios C and Koudoumas E 2002 *J. Phys. Chem. A* **106** 2838
[43] Liu Y, He S, Zhou L X, Chen Q, Zhao Y W, Sun T, Shen X C, Yu T, Lv H and Xu H F 2023 *J. Opt. Soc. Am. B* **40** 1851
[44] Rott F, Reduzzi M, Schnappinger T, Kobayashi Y, Chang K F, Timmers H, Neumark D M, Vivie-Riedle R D and Leone S R 2021 *Struct. Dyn.* **8** 034104

[45] Zhou L X, Liu Y, He S, Gao D S, Shen X C, Chen Q, Yu T, Lv H and Xu H F 2022 *Chin. Phys. B* **31** 028202

[46] Ammosov M V, Delone N B and Krainov V P 1986 *Sov. Phys. JETP* **64** 1191

[47] Perelomov A M, Popov V S and Terent'ev M V 1966 *J. Exptl. Theoret. Phys.* **50** 1393

[48] Keldysh L V 1965 *Sov. Phys. JETP* **20** 1307

[49] Chadwick D, Frost D C, Katrib A, McDowell C A and McLean R A N 1972 *Can. J. Chem.* **50** 2642

[50] McCracken G A, Kaldun A, Liekhus-Schmaltz C and Bucksbaum P H 2017 *J. Chem. Phys.* **147** 124308

[51] Yan J L, Chen J T, Liu D, Lian Y, Yao H Q, Wu Q, Lv H, Yan B and Xu H F 2024 *Chin. J. Chem. Phys.* **37** 737

[52] Humpert H J, Schwier H, Hippler R and Lutz H O 1985 *Phys. Rev. A* **32** 3787

[53] Trippenbach M, Rzaewski K and Grobe R 1988 *Phys. Rev. A* **37** 4194

[54] Nandor N J, Walker M A and Woerkom L D V 1998 *J. Phys. B: At. Mol. Opt. Phys.* **31** 4617

[55] Korneev Ph A, Popruzhenko S V, Goreslavski S P, Yan T M, Bauer D, Becker W, Kübel M, Kling M F, Rödel C, Wünsche M and Paulus G G 2012 *Phys. Rev. Lett.* **108** 223601

[56] Li M, Liu Y Q, Liu H, Yang Y D, Yuan J L, Liu X R, Deng R K, Wu C Y and Gong Q H 2012 *Phys. Rev. A* **85** 013414